Influence of interface reconstruction on the formation and superconductive properties of metastable Pb-Ga alloy films

Eun Ju Moon, Mustafa M. Özer, James R. Thompson, and Hanno H. Weitering

Phys. Rev. B **84**, 235434 — Published 21 December 2011

DOI: 10.1103/PhysRevB.84.235434

Influence of Interface Reconstruction on the Formation and Superconductive Properties of metastable Pb-Ga Alloy Films

Eun Ju Moon,[1] Mustafa M. Özer,[1,2] James R. Thompson,[1,2] and Hanno H. Weitering[1,2,*]

[1]*Department of Physics and Astronomy, The University of Tennessee, Knoxville, TN 37996, USA*
[2]*Materials Science and Technology Division, Oak Ridge National Laboratory, Oak Ridge, TN 37831, USA*

(Dated: October 6, 2011)

We show that the growth, composition, and superconductive properties of ultrathin $Pb_{1-x}Ga_x$ alloy films depend strongly on the atomic structure of the substrate interface. Whereas alloy films on the Si(111)-(7×7) surface grow in multilayers, reminiscent of the quantum growth phenomenon observed in pure Pb layers, alloy films on the Si(111)-$(\sqrt{3}\times\sqrt{3})R30°$-Pb and Si(111)-$(\sqrt{3}\times\sqrt{3})R30°$-Ga interfaces gradually switch to classical layer-by-layer growth. The (7×7) interface is unique in that it enables formation of atomically smooth alloy films containing up to 6% of Ga, which is far beyond the solid solubility limit. In contrast, the $(\sqrt{3}\times\sqrt{3})$ interfaces promote phase separation. The contrasting influences of these interfaces are also reflected by their superconductive properties, most notably by the differences in the critical current density, exceeding more than one order of magnitude.

PACS numbers:

I. INTRODUCTION

The substrate plays a critical role in thin film heteroepitaxy. Thin film growth is determined by a variety of thermodynamic and kinetic parameters, many of which can be related to -and in some cases controlled by- the atomic scale structure and mesoscopic morphology of the starting substrate. By choosing a proper substrate, the structure, morphology and properties of a thin film material can often be engineered to desirable qualities. Arguably, the most interesting cases are those in which deposited atoms self-organize into a novel nanophase material. Interesting examples include the formation of optically active quantum dots and quantum-dot superlattices in Si/Ge[1] and PbSe/PbTe heteroepitaxy,[2] metallic nanowires in silicide heteroepitaxy,[3,4] or the formation of atomically smooth metal films on semiconductor surfaces.[5,6] While the formation of wires and dots appears to be driven by a classical strain relaxation mechanism, the formation of atomically-smooth metal films is often driven by quantum-mechanical confinement.[6,7] The substrate is essential in both cases because it determines the strain energy and quantum mechanical boundary conditions of the films.[6–10]

Atomically-clean substrate surfaces are often reconstructed. The surface reconstruction can be altered or eliminated by deposition of (sub)-monolayer (ML) amounts of a third species, prior to thin film deposition. Such template modification can facilitate smooth layer growth through surfactant[11,12] or interfactant action[13] or it can be used to control the band offset or Schottky barrier at the interface.[8,14,15] In this report, we show how the modification of a Si(111)-(7×7) template into a Si(111)-$(\sqrt{3}\times\sqrt{3})R30°$ template prior to the deposition of an ultrathin quantum-confined $Pb_{1-x}Ga_x$ alloy film ($x\approx0.06$)[16] significantly changes the kinetic solubility of the Ga, attenuates the robustness of the bilayer quantum growth and produces a dramatic contrast in the superconducting critical state properties. The results underscore the unique role of the quantum growth morphology in establishing robust critical currents at the nanoscale and furthermore show how template modification or interface engineering might be used to alter self-organization phenomena and collective properties in the nanophase.

II. EXPERIMENTAL PROCEDURES

$Pb_{1-x}Ga_x$ alloy films were grown at ∼120 K in ultrahigh vacuum (UHV) by co-deposition of Pb and Ga onto three different templates, namely the Si(111)-(7×7), Si(111)-$(\sqrt{3}\times\sqrt{3})R30°$-Pb, and Si(111)-$(\sqrt{3}\times\sqrt{3})R30°$-Ga interfaces (henceforth (7×7), $\sqrt{3}$-Pb and $\sqrt{3}$-Ga templates, respectively). The films were postannealed in UHV at about 230 K to 250 K so as to obtain atomically-smooth morphologies.[6] Low-energy electron diffraction patterns and step-height measurements in scanning tunneling microscopy (STM) studies indicate that the films grow in the fcc (111) orientation with the [110] crystallographic direction parallel to that of the substrate. The nominal Ga content of the alloys films was (6 ± 1)%, following our earlier thickness-dependent study of PbGa alloy formation on (7×7).[16] Film thicknesses were fixed at about 8 ML.[17] We employed established procedures for calibrating the deposition rate of Pb[18] and that of Ga.[16,19] The $\sqrt{3}$-Pb interface was prepared by depositing 1/3 ML of Pb onto Si(111)-(7×7) at 250°C, following the procedures by Ganz *et al.*[20] The $\sqrt{3}$-Ga phase was prepared by depositing approximately 1.5 ML of Ga onto clean Si(111)-(7×7) at room temperature. The substrate was subsequently heated at 650°C to evaporate the excess Ga until the $(\sqrt{3}\times\sqrt{3})$ low energy electron diffraction pattern was fully developed with 1/3 ML of Ga remaining on the surface. The existence of the $\sqrt{3}$ phases was

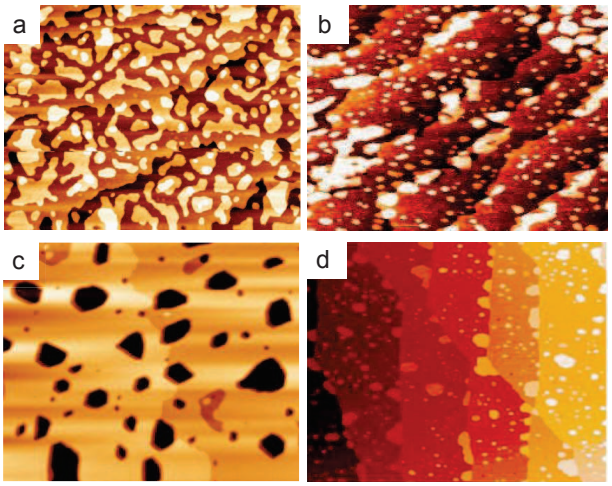

FIG. 1: (Color online) STM images of a 8-ML $Pb_{0.94}Ga_{0.06}$ alloy film on the $\sqrt{3}$-Ga interface (a) and $\sqrt{3}$-Pb interface (b), showing atomically smooth mesas. The image sizes are (500×300) nm^2. (c) STM image of an 8 ML $Pb_{0.94}Ga_{0.06}$ alloy film on Si(111)-(7×7) showing an atomically smooth film with large 6-ML deep holes. The image size is (700×600) nm^2. (d) STM image of a 8 ML pure Pb film. The image size is (700×600) nm^2.[21] The color contrasts in all images reflect local height differences between atomically-flat film areas with the brightest regions representing the tallest plateaus.

verified with STM.

The superconductive properties of the alloy films on the (7×7) and $\sqrt{3}$ interfaces were investigated ex-situ by SQUID magnetometry, following the procedures of Özer *et al.*[21] Briefly, the samples were sealed with an amorphous Ge capping layer deposited at ∼120 K, prior to removal from the UHV system. STM data verified that the atomically smooth morphology of the metal films remains preserved under the capping layer, at least up to room temperature. The capped samples were subsequently inserted into the SQUID magnetometer for contact-free *dc* and *ac* measurements, with all magnetic fields applied perpendicular to the surface.

III. RESULTS AND DISCUSSION

Thin Film Growth— Pb and Ga are completely immiscible in bulk form. However, in the ultrathin quantum-size regime, atomically-smooth $Pb_{0.94}Ga_{0.06}$ alloy films can be stabilized on Si(111)-(7×7)[16]. Here, we investigate how the solid solubility of Ga in Pb and resulting film morphology are qualitatively affected by the nature of the substrate interface. To address the Ga solubility in Pb, we measured the intensity ratio of the Ga $2p_{1/2}$ and Pb $4f_{7/2}$ core levels in XPS (not shown). For 8 ML thick $Pb_{1-x}Ga_x$ alloy films on (7×7), the intensity ratio equals 0.06 after annealing and smoothening of the film at ∼250 K. This ratio is consistent with a nominal Ga percentage of about 6%.[16] On the other hand, for the alloy films formed on the $\sqrt{3}$-Ga and $\sqrt{3}$-Pb interfaces, this ratio dropped to 0.01, indicating that Ga diffuses toward the buried interface. Films on the $\sqrt{3}$ interfaces are thus depleted of Ga. The short mean free path of the Ga $2p_{1/2}$ photoelectrons, however, does not allow us to determine and compare the exact doping profiles near the buried interfaces. From now on, the alloy films grown on each of these interfaces will be denoted by $Pb_{0.94}Ga_{0.06}$, reflecting only their nominal Pb and Ga contents without reference to the actual dopant distributions.[22]

Figs. 1(a) and (b) display STM images of $Pb_{0.94}Ga_{0.06}$ alloy films deposited onto the $\sqrt{3}$-Ga and $\sqrt{3}$-Pb interfaces, respectively. The nominal coverage is 8 ML. Fig. 1(a) shows 1 ML tall islands on an otherwise flat film indicating that the system assumes the classical layer-by-layer growth mode. Fig. 1(b), on the other hand, reveals a coexistence of monolayer- and bilayer-high islands on the $\sqrt{3}$-Pb template, suggesting that classical and quantum growth modes compete. Finally, alloy films on Si(111)-(7×7) grow in multilayers, which is characteristic of strong quantum size effects on the growth mode.[16]

The 8 ML alloys films on (7×7) are uniquely characterized by their much higher distributed Ga content and by the presence of large 6-ML deep holes, shown in Fig. 1(c). The lateral dimensions of the holes can easily reach hundred nanometers. 6 ML turns out to be the minimum thickness for achieving atomic smoothness.[16] Subsequent stable layer thicknesses follow a bilayer pattern up to 12 ML, indicative of strong quantum size effects on the growth.[6,16] Following the procedure in Ref. 16, we determined that the film thickness inside the holes is 2 ML so that the total film thickness in regions between these "blind" holes equals 8 ML. For the sake of completeness, we show the morphology of a 8 ML pure Pb film deposited on (7×7)[21,23] in Fig. 1(d). The characteristic bilayer growth mode is evident from the 2 ML tall mesas that decorate the surface (and from the absence of 1 ML tall mesas and voids). However, pure Pb films do not exhibit the 6 ML deep holes seen in the alloy films on (7×7). As we shall see, these contrasting morphologies have significant consequences for the maximum supercurrent densities that these quantum films can sustain.

The growth observations are summarized in Table I. We tentatively conclude that the use of the (7×7) template leads to stronger quantum-size effects on the film morphology and enhances the kinetic solubility of Ga in Pb. By contrast, the use of the $\sqrt{3}$-Pb and $\sqrt{3}$-Ga tem-

TABLE I: Observed growth modes of Pb and $Pb_{0.94}Ga_{0.06}$ alloys on the (7×7), $\sqrt{3}$-Pb, and $\sqrt{3}$-Ga interfaces.

	(7×7)	$\sqrt{3}$-Pb	$\sqrt{3}$-Ga
Pure Pb film	Bi-layer	Bi-layer[a]	×
PbGa alloy film	Bi-layer	Single/Bi- layer	Single layer

[a]Ref.21

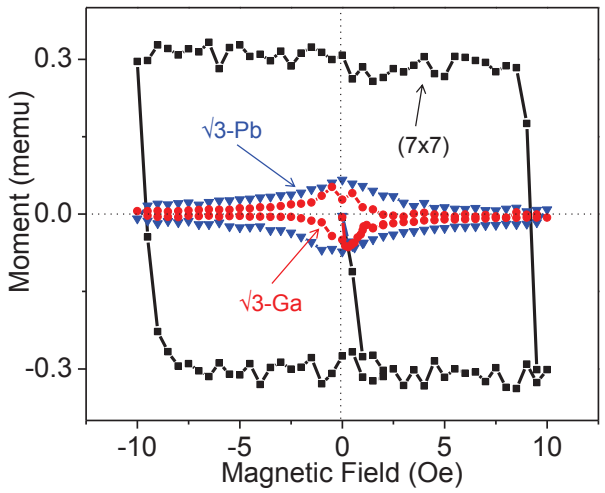

FIG. 2: (Color online) *dc* Magnetization loops at 2 K of 8 ML thick $Pb_{0.94}Ga_{0.06}$ alloy films, grown on Si(111)-7 × 7 (■), $\sqrt{3}$-Pb (▼), and $\sqrt{3}$-Ga (●).

plates reduces the robustness of the quantum growth and lowers the solubility of Ga in Pb. Evidently, films on the $\sqrt{3}$ interfaces exhibit more classical characteristics where the reduced Ga solubility is more in line with the classical phase diagram. The apparent quantum-versus-classical nature of the alloy films on the (7 × 7) and $\sqrt{3}$ interfaces could perhaps be attributed to differences in Schottky barrier height (or confinement barrier) at the substrate interface where the (7 × 7) interfaces usually exhibit higher Schottky barriers.[8,15,24] Alternatively, the Ga concentration gradient for the $\sqrt{3}$ interfaces might also weaken the vertical quantum interference that is necessary for establishing quantum growth.[25] The ramifications of the template choice on the superconductive properties will be discussed next.

Superconducting Properties— The superconducting transitions at zero *dc* magnetic field are very sharp (not shown). The T_c values of the 8 ML alloy films on the (7 × 7), $\sqrt{3}$-Pb, and $\sqrt{3}$-Ga templates exhibit only marginal differences (5.9 K, 5.8 K, and 5.7 K, respectively). However, the contrasting film morphologies on the different templates have dramatic consequences for the critical current densities J_c. Fig. 2 shows the hysteretic *dc* magnetic moments m of the alloy films grown on (7 × 7), $\sqrt{3}$-Pb and $\sqrt{3}$-Ga as a function of the applied magnetic field H, recorded at 2 K. The magnetic moments are produced by the superconductive currents that screen the changes of the applied *dc* magnetic field with $m \propto J_c$. Because the shape and magnetic volumes of all samples are very similar, the different moments in Fig. 2 indicate large differences in the critical current densities that these films can support as a function of the magnetic field.

The critical current densities at 2 K and 5 Oe *dc* field are obtained from the magnetic moments in Fig. 2 via the Bean critical-state relation[26] $J_c = 30m/Vr$ where V is the volume of the film and r is the macroscopic radius of the circulating currents, which we set equal to the radius of the sample (≈ 0.15 cm). J_c amounts to 4.4, 0.4, and 0.1 MA/cm^2 for the alloy films on the (7 × 7), $\sqrt{3}$-Pb, and $\sqrt{3}$-Ga interfaces, respectively. The *dc* magnetization loops of the Pb-Ga alloys on (7 × 7) are almost perfectly rectangular; *i.e.* they are "hard" superconductors.[26] Evidently, these films behave as ideal Bean-type superconductors, implying strong vortex pinning. In contrast, the much smaller J_c values and "soft" magnetization loops of the alloy films on the $\sqrt{3}$ interfaces indicate weak pinning where J_c rapidly decreases as a function of the magnetic field.

In the case of slightly underdosed pure Pb films on (7 × 7), the vortex pins have been associated with the presence of 2 ML-deep blind holes with diameters that are of the order of the superconducting coherence length.[27] The hole depths in those films are perfectly uniform and result from the strongly preferred bi-layer growth. They determine the length over which the vortex is pinned, and consequently, the critical current density. For the alloy films on (7 × 7), the holes are 6 ML deep. According to the relation $J_c \propto \Delta(d)/d$ in Ref. 27, this implies even stronger vortex pinning in the alloy films with J_c values exceeding those of pure Pb films[21,27] by about a factor of three (d is the film thickness and $\Delta(d)$ is the hole depth). Indeed, from the *dc* magnetization measurements in Fig. 2 and the temperature-dependent *ac* magnetic data discussed below, we find that the critical current densities in the alloy film on (7 × 7) exceed those of pure Pb films on (7 × 7) by a factor of 2 to 3.

The absence of deep holes for the $\sqrt{3}$ interfaces is undoubtedly the main reason for their much lower critical current densities. Note, however, that the critical current density of the $\sqrt{3}$-Pb interface exceeds that of $\sqrt{3}$-Ga by about a factor of four (2 K, 5 Oe). This suggests that the interface still plays a significant role in determining the critical state properties of the films when the morphology contrasts of the films are much more subtle. Note that *dc* moments strongly depend on the macroscopic connectivity of the critical currents flowing along the perimeter of the sample and hence it is possible that the contrasts in *dc* magnetization are due in part to differences in sample quality. However, as will be shown shortly, the observed trends in the dc moments for the three different interfaces do reflect the intrinsic critical-state properties of these thin films.

To acquire complementary values of the critical current density and its full temperature dependence, we measured the *ac* magnetic response ($m = m' + im''$) as a function of temperature at various *ac* driving amplitudes h_{ac} superimposed on a 5 Oe *dc* magnetic field. The *ac* response of a thin superconducting film depends on the critical current density and thickness of the film but is independent of the macroscopic connectivity. The frequency of the *ac* field was 100 Hz for all *ac* measurements. The m'' values of the (7 × 7) and $\sqrt{3}$-Ga interfaces are shown in Fig. 3(a) and (b), respectively. Notice the qualitative differences for the materials grown on these

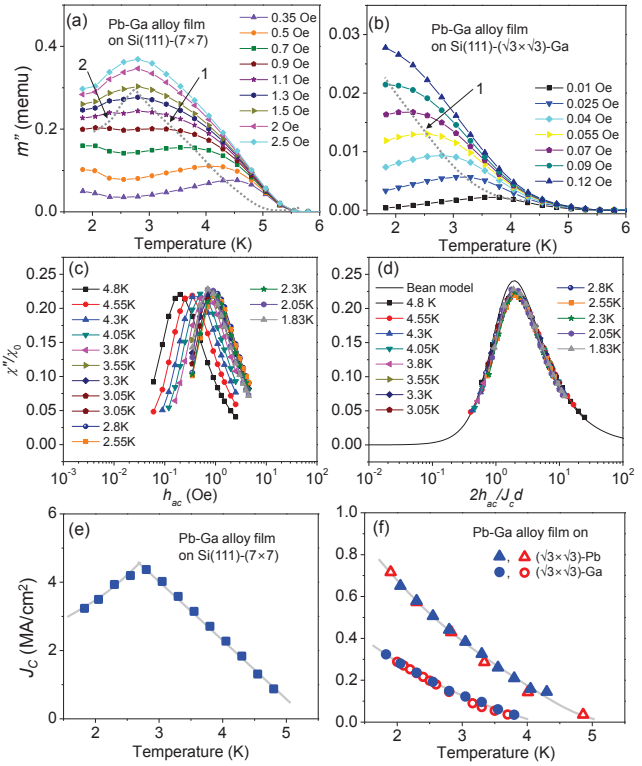

FIG. 3: (Color online) Panels (a) and (b): Imaginary part m'' of the ac magnetic response of 8 ML thick alloy films grown on the(7×7) and $\sqrt{3}$-Ga interface, respectively, measured in 5 Oe dc field. Dotted gray lines trace the locations of the peak positions in m''. Panels (c) and (d): Normalized χ'' versus h_{ac} for the the (7×7) interface and its fitting to the critical state model, respectively, where J_c is obtained as a scaling parameter. χ_o is the susceptibility of the fully screened critical state measured at 2 K and 5 Oe. Panels (e) and (f): Filled symbols mark the critical current densities as a function of temperature in 5 Oe dc field, obtained from fitting χ'' to the critical state model.[28] The open symbols in panel (f) are data points obtained from the condition $J_c = 1.03h_{ac}/d$ at the peak position in m''.[27] The solid lines serve as guides to the eye.

two interfaces: m'' of the (7×7) interface shows an intriguing double peak structure at moderate driving amplitudes, as indicated by the dotted gray lines, whereas m'' of the $\sqrt{3}$-Ga interface reveals a single peak shifting monotonically toward lower temperature with increasing driving amplitude. The $\sqrt{3}$-Pb interface exhibits qualitatively similar behavior (not shown). According to the relation $J_c = 1.03h_{ac}/d$,[27] which is valid at the peak position, this monotonic shift implies a monotonic increase of J_c as the temperature is lowered.

In Ref. 16 we have shown that the double peak feature of the (7×7) interface is related to a highly unusual non-monotonic $J_c(T)$ dependence as J_c initially *increases* with temperature. Here, $J_c(T)$ is obtained by fitting the normalized susceptibility $\chi''/\chi_0 = [m''/(Vh_{ac})]/\chi_0$ to the critical state model,[16,28] as illustrated in Figs. 3(c) and 3(d) for the (7×7) interface. The quantity χ_0 is the magnitude of the in-phase susceptibility $\chi' = m'/(Vh_{ac})$ corresponding to complete screening, which was measured at 2 K with $h_{ac} = 10$ mOe in 5 Oe dc field. Fig. 3(c) is in essence an alternative representation of the data in Fig. 3(a), showing χ'' versus h_{ac} for different temperatures. When these χ'' isotherms are scaled as a function of $h_{ac}/J_c d$, one observes that all data points collapse onto the χ'' of the critical state model, as shown in Fig. 3(d). In this process, $J_c(T)$ is obtained as the scaling parameter that produces the best fit to the critical state model. Figs. 3(e) and 3(f) show $J_c(T)$ for the (7×7) interface and both $\sqrt{3}$ interfaces, respectively.

Following Ref. 16, the unusual occurence of a maximum in $J_c(T)$ of the (7×7) interface (Fig. 3(e)) is attributed to the unique presence of the 6-ML deep holes and a weakened vortex pinning below 2.8 K as the 2-ML thick films at the bottom of the holes presumably become superconducting. Hence, alloy films grown on (7×7) appear to have totally unique pinning properties. Quantitatively, the ac study yields J_c values of 3.5 MA/cm^2, 0.65 MA/cm^2 and 0.28 MA/cm^2 at 2 K and 5 Oe dc field, for the (7×7), $\sqrt{3}$-Pb and $\sqrt{3}$-Ga interfaces, respectively. The contrast between the (7×7) and $\sqrt{3}$ interfaces is

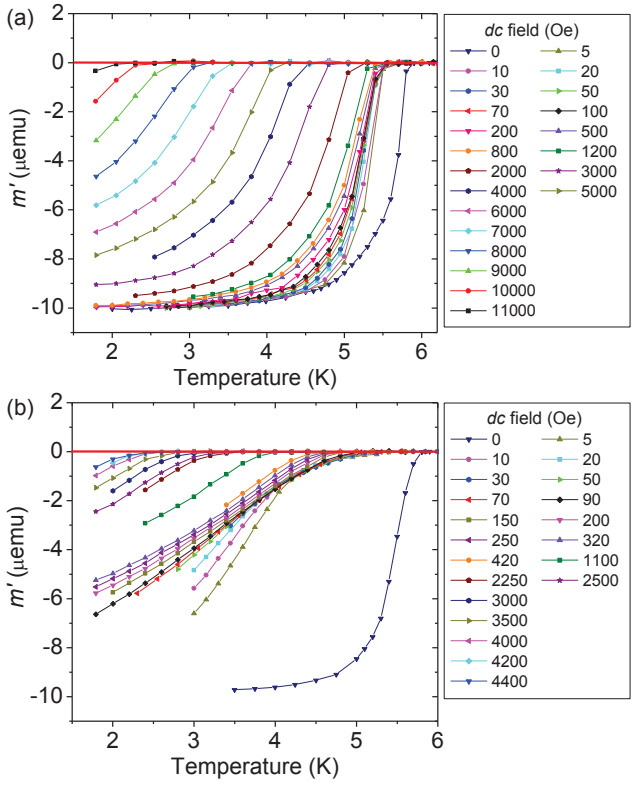

FIG. 4: (Color online) Real part of the ac magnetization (m') versus T in various dc magnetic fields for the (a) $(7 \times 7)$and (b) $\sqrt{3}$-Ga interface. The diamagnetic onsets indicate the critical temperature for a given dc field or, alternatively, the critical magnetic field at that same temperature, $H_{c2}(T)$.

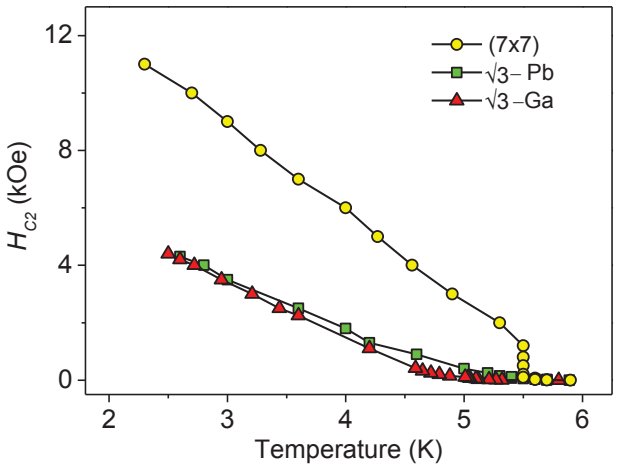

FIG. 5: (Color online) $H_{c2}(T)$ values of $Pb_{0.94}Ga_{0.06}$ alloy films on the (7 × 7), $\sqrt{3}$-Pb, and $\sqrt{3}$-Ga templates. The corresponding T_c values are 5.9 K, 5.8 K, and 5.7 K, respectively. Nominal coverages are 8 ML.

even larger at 2.8 K where J_c of (7 × 7) reaches its maximum, exceeding that of $\sqrt{3}$-Ga by about a factor of 30. Again, this dramatic difference in critical current density of more than one order of magnitude highlights the contrasting vortex-pinning-potential landscape for the (7 × 7) versus $\sqrt{3}$ interfaces. The origin of the different J_c values for the two different $\sqrt{3}$ interfaces is less clear. They differ by a factor 2.3 or higher, depending on the temperature, which is significantly larger than what might be expected from their different growth morphologies (1 ML versus 2 ML steps). Note that the critical current densities obtained from the *ac* and *dc* measurements at 2 K and 5 Oe have comparable magnitudes, indicating strong macroscopic phase coherence in these 8 ML-thick films with macroscopic circulating supercurrents that are of the order of 150 mA in the case of (7 × 7).

Finally, we explore the phase boundaries of the superconducting alloys in the presence of a large *dc* magnetic field. The upper critical field $H_{c2}(T)$ of the films was determined from the onset of diamagnetic screening (i.e., m') as a function of temperature in different *dc* fields. A 10 mOe *ac* probing amplitude was superimposed on the out-of-plane *dc* fields. The real parts of the magnetizations (m') of the (7 × 7) and $\sqrt{3}$-Ga interfaces are shown in Figs. 4(a) and (b). Fig. 5 shows corresponding $H_{c2}(T)$ data of the alloy films on all three templates. At low temperature, the upper critical field of the three alloy films decreases linearly with temperature, as given by the Ginzburg-Landau theory. However, in the close vicinity of T_c, the $H_{c2}(T)$ data deviate significantly from the linear Ginzburg-Landau behavior, showing a 'hockey stick" profile for the $\sqrt{3}$ interfaces and a step-like increase near 5.5 K for the (7 × 7) interface. Only in the (7 × 7) case does the linear Ginzburg-Landau-like segment extrapolate to T_c at 5.9 K.

The upper critical field is related to the carrier mean free path l via the Ginzburg-Landau expression $H_{c2}(T) = \Phi_0/2\pi\xi_{GL}^2(T)$ and the interpolation formula $\xi_{GL} = 0.739(\xi_0^{-2}+0.882(\xi_0 l)^{-1})^{-1/2}(1-T/T_c)^{-1/2}$.[29] Here, ξ_{GL} is the Ginzburg-Landau coherence length of the films, Φ_0 the magnetic flux quantum, and ξ_0 is the normalized BCS coherence length.[30] From the upper critical field at 2.6 K, we obtain the scattering mean free paths of the $Pb_{0.94}Ga_{0.06}$ alloys on both $\sqrt{3}$ and (7 × 7) interfaces. They were determined to be 62 Å and 27 Å, respectively, which amounts to 2.7× and 1.2× the film thickness (8 ML). The reduced scattering for the $\sqrt{3}$ interfaces is consistent with the notion that the alloy films on the $\sqrt{3}$ interfaces are depleted of Ga and, consequently, there are fewer charged impurity scatterers.[31] Qualitatively, however, the large deep holes on the (7 × 7) interface can also be expected to contribute to scattering of carriers, perhaps significantly so.

IV. CONCLUSION

The growth, composition, and superconductive properties of metastable $Pb_{0.94}Ga_{0.06}$ alloy films in the ultrathin quantum-size regime are strongly affected by the atomic scale nature of the starting interface, suggesting a possibility for tuning the assembly and emergent properties of surface based nanostructures via template modification or passivation.

V. ACKNOWLEDGEMENT

This research was supported by the U.S. Department of Energy, Basic Energy Sciences, Materials Sciences and Engineering Division (M.M.O., J.R.T., and H.H.W.) and by the National Science Foundation under contract No. DMR 0906025(E.J.M.).

* Electronic address: hanno@utk.edu

[1] J.L. Liu, G. Jin, Y.S. Tang, Y.H. Luo, K.L. Wang, and D.P. Yu, Appl. Phys. Lett. **76**, 586 (2000).
[2] G. Springholz, V. Holy, M. Pinczolits, and G. Bauer, Science **282**, 734 (1998).
[3] C. Preinesberger, S. Vandré, T. Kalka, and M. Dähne-Prietsch, J. Phys. D: Appl. Phys, **31**, L43 (1998).
[4] C. Zeng, P.R.C. Kent, T. -H. Kim, A.P. Li, and H.H. Weitering, Nat. Mat. **7**, 539 (2008).
[5] A.R. Smith, K.-J. Chao, Q. Niu, and C. -K. Shih, Science **273**, 226 (1996).
[6] M.M. Özer, C.-Z. Wang, Z. Zhang, and H.H. Weitering, J.

Low Temp. Phys. **157**, 221 (2009).
[7] Z.Y. Zhang, Q. Niu, and C.-K. Shih, Phys. Rev. Lett. **80**, 5381 (1998).
[8] D.A. Ricci, T. Miller, and T.-C. Chiang, Phys. Rev. Lett. **93**, 136801 (2004); **95**, 266101 (2005).
[9] N.J. Speer, S.-J. Tang, T. Miller, and T.-C. Chiang, Science **314**, 804, (2006).
[10] V. Yeh, L. Berbil-Bautista, C.Z. Wang, K.M. Ho, and M.C. Tringides, Phys. Rev. Lett. **85**, 5158 (2000).
[11] J. Vrijmoeth, H.A. van der Vegt, J.A. Meyer, E. Vlieg, and R.J. Behm, Phys. Rev. Lett. **72**, 3843 (1994).
[12] M. Horn von Hoegen, App. Phys. A **59**, 503 (1994).
[13] M. Jałochowski and E. Bauer, J. Appl. Phys. **63**, 4501 (1988).
[14] R.T. Tung, Phys. Rev. Lett. **52**, 461 (1984).
[15] D.R. Heslinga, H.H. Weitering, D.P. van der Werf, T.M. Klapwijk, and T. Hibma, Phys. Rev. Lett. **64**, 1589 (1990).
[16] E.J. Moon, M.M. Özer, Y. Jia, G. Duscher, J.R. Thompson, Z.Y. Zhang, and H.H. Weitering, Phys. Rev. B **84**, 125415 (2011).
[17] By fixing the film thickness and Ga concentration, we focus exclusively on the role of the template. 8 ML is also the minimum thickness showing striking contrasts in morphology and critical state properties of superconducting thin films grown on different interface reconstructions.
[18] M. Hupalo, J. Schmalian, and M.C. Tringides, Phys. Rev. Lett. **90**, 216106 (2003).
[19] P.C. Snijders, E.J. Moon, C. González, S. Rogge, J. Ortega, F. Flores, and H.H. Weitering, Phys. Rev. Lett. **99**, 116102 (2007).
[20] E. Ganz, H. Ing-Shouh, X. Fulin, S.K. Theiss, and J. Golovchenko, Surf. Sci. **257**, 259 (1991).
[21] M.M. Özer, J.R. Thompson, and H.H. Weitering, Phys. Rev. B **74**, 235427 (2006).
[22] The 1/3 ML of Ga(Pb) of the $\sqrt{3}$-Ga(Pb) interface layer is excluded in this definition of 'nominal Ga(Pb) content".
[23] M.M. Özer, Y. Jia, B. Wu, Z.Y. Zhang, and H.H. Weitering, Phys. Rev. B **72**, 113409 (2005).
[24] H.H. Weitering, J.P. Sullivan, R.J. Carolissen, R. Perez-Sandoz, W.R. Graham, and R.T. Tung, J. Appl. Phys. **79**, 7820 (1996).
[25] One cannot rule out the possibility that quantum size effects do remain strong in the case of the $\sqrt{3}$ interfaces but that the kinetic pathway for establishing the characteristic quantum-mechanical bilayer growth mode was bypassed inadvertently with the low-temperature deposition and postannealing synthesis.
[26] C.P. Bean, Phys. Rev. Lett. **8**, 250 (1962).
[27] M.M. Özer, J.R. Thompson, and H.H. Weitering, Nature Phys. **2**, 173 (2006).
[28] J.R. Clem and A. Sanchez, Phys. Rev. B **50**, 9355 (1994).
[29] T.P. Orlando, E.J. McNiff, Jr., S. Foner, and M.R. Beasley, Phys. Rev. B **19**, 4545 (1979).
[30] $\xi_0 = \xi^{Pb} \times T_c^{Pb}/T_c$ where ξ^{Pb} is the BCS coherence length of bulk Pb; see also Ref. 27.
[31] Ga atoms in Pb act as hole-dopants (Ref. 16). Accordingly, they are also charged impurities; see also M.M. Özer, Y. Jia, Z.Y. Zhang, J.R. Thompson, and H.H. Weitering, Science **316**, 1594 (2007).